

Supplementary Materials for:

**Methane accumulation affected by particulate organic carbon in
upper Yangtze deep valley dammed cascade reservoirs, China**

Yuanyuan Zhang^{1,2}, Youheng Su^{2,3}, Zhe Li^{1,2*}, Shuhui Guo⁴, Lunhui Lu^{1,2},

Bin Zhang², Yu Qin³

¹ College of Resources and Environment, Chongqing School, University of Chinese Academy of Sciences, 400714, Chongqing, China

² CAS Key Lab of Reservoir Environment, Chongqing Institute of Green and Intelligent Technology, Chinese Academy of Sciences, 400714, Chongqing, China

³ College of River and Ocean Engineering, Chongqing Jiaotong University, 400074, Chongqing, China

⁴ Foreign Environmental Cooperation Center, Ministry of Ecology and Environment of the People's Republic of China, 100035, Beijing, China

* Corresponding author. Email: lizhe@cigit.ac.cn

Supplementary Materials Contain:

11 Pages (Page S1-11)

11 Figures (Figure S1-11)

1 Table (Table S1)

S1.1 Detailed methods for hydraulic retention time and mass balance approach of the POC and CH₄ in the XLD and XJB reservoirs

Hydraulic retention time (HRT, the time required for the river water to be completely replaced per kilometer) was relative to water level and flow, distance. The relationships among the water level, section distance, and reservoir capacity were obtained by a hydraulic model. The inflow of the XJB reservoir was as the flow of all sections in the XJB reservoir because there were no large tributaries. Additionally, the discharge of the XLD reservoir was the flow of all sections in the XLD reservoir due to the sampling sites close to the dam. HRT is calculated by following:

$$F(w, f, x) = \frac{dV(w, x)}{fdx} \quad (1)$$

where w is the water level before the dam (m), x is the distance from the sampling sites to the end of the dam (m), f is the water flow (m³/s), V is the cumulative reservoir capacity (the function of the water level and distance) and F is the hydraulic retention time per kilometer (d/km).

In addition, the mass balance approach of the POC and CH₄ was used in both reservoirs to explore hydrological effects on CH₄ dynamics. The B10 and X2 sampling sections were the first sites under the XLD and XJB reservoirs, respectively, which were considered interceptions of the control section for the XJB reservoir because the water column was fully mixed. The interception of POC in the XJB reservoir was calculated monthly and the input/output of POC mass is estimated during sampling as follows:

$$\Delta POC flux_j = 0.0864 \times \sum_i POC_{ij} \times flow_{ij} \quad (2)$$

$$\sum \Delta POC flux = \sum_j \Delta POC flux_j \quad (3)$$

where $\Delta POC flux_j$ is the mass balance of POC in the j th month, positive with input and negative with output (Tg/d), POC_{ij} is the concentration of POC at the i th sampling section in the j th month (mg/L), $flow_{ij}$ is the water flow at the i th sampling

section in the j th month (m^3/s), and $\sum \Delta POCflux$ is the total mass balance of POC in each month (Tg/d).

The CH_4 concentration in water and flux of CH_4 air-water are first calculated by the standard method, which was widely applied in freshwater research (Unesco/Iha, 2010). Although CH_4 oxidation can reduce the CH_4 concentration, it is difficult to compare with CH_4 production in water. Therefore, the mass balance of CH_4 in the XJB reservoir can reflect the variation trend of CH_4 production, which is calculated as:

$$\Delta CH_4 flux_k = 1.3824 \times 10^{-3} \sum_i CH_{4ik} \times flow_{ik} + 3.84 \times 10^{-7} \sum_j A_{jk} \times CH_4 flux_{jk} \quad (4)$$

$$\sum \Delta CH_4 flux = \sum_k \Delta CH_4 flux_k \quad (5)$$

where $\Delta CH_4 flux_k$ is the mass balance of CH_4 in the k th month (Tg/d), CH_{4ik} is the concentration of CH_4 at the i th sampling section in the k th month ($\mu\text{mol}/\text{L}$), $flow_{ik}$ is the water flow at the i th sampling section in the k th month (m^3/s), A_{jk} is the water surface area at the j th sampling site in the k th month (m^2), $CH_4 flux_{jk}$ is the air-water flux of CH_4 at the j th sampling site in the k th month ($\text{mmol}/\text{m}^2/\text{h}$), and $\sum \Delta CH_4 flux$ is the total mass balance in each month (Tg/d).

S1.2 Spatial and temporal variations in autochthonous and terrestrial POC concentrations

The concentrations of autochthonous POC in all water columns from January to July 2018 ($0.13 \pm 0.08 \text{ mg}/\text{L}$, SD, $n=103$) were higher than those from September 2018 to January 2019 ($0.07 \pm 0.03 \text{ mg}/\text{L}$, SD, $n=78$, Figure S5). Additionally, the peak value of autochthonous POC in the XLD reservoir was later found than that in the XJB reservoir. The concentrations of autochthonous POC in the surface and bottom water did not show significant differences except for higher autochthonous POC concentrations in May from the XLD reservoir (Figure S5A, S5B). Autochthonous POC largely displayed an increasing trend before the dam. The highest peak value of terrestrial POC was found in March ($0.85 \pm 0.59 \text{ mg}/\text{L}$, SD, n

=26), which was much higher than the annual average level (0.24 ± 0.36 mg/L, SD, $n=181$, Figure S5). The concentrations of terrestrial POC from bottom water in March, which was well mixed were higher than those in surface water, and the terrestrial POC concentration from bottom water at approximately 50 km suddenly decreased in March (Figure S5A, S5B), which may reveal the sedimentation of particulate matter. The peak value of terrestrial POC was found before the XJB dam in July, which was similar to that in March. This may indicate that the input of terrestrial POC in the XJB reservoir during the flood period may be mainly derived from resuspended particulate matter rather than from upstream particulate matter.

S2. Figures

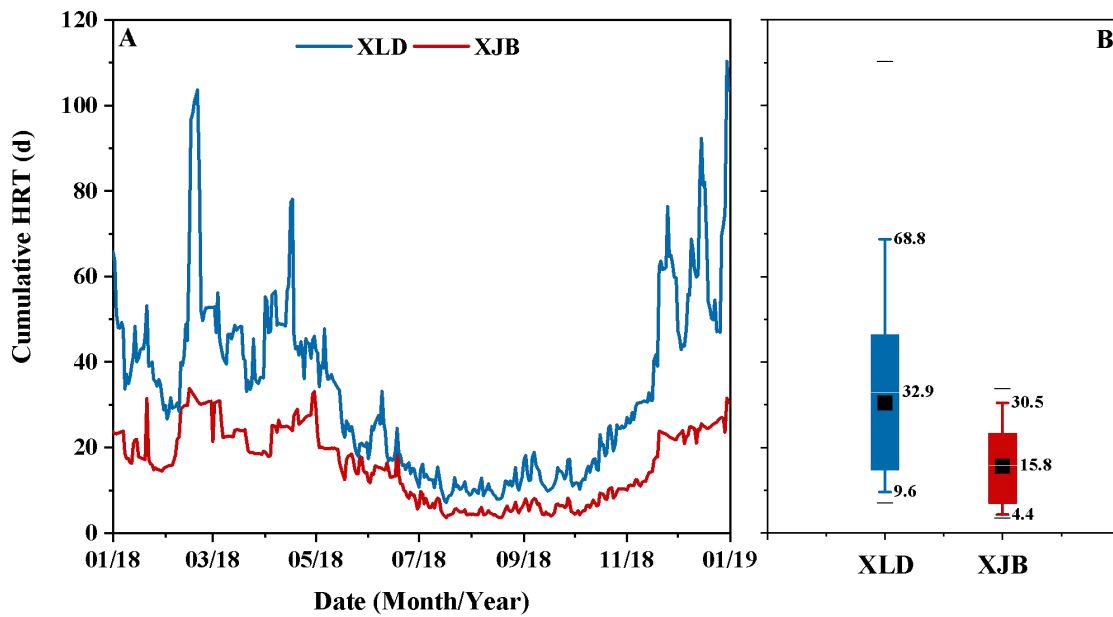


Figure S1. A) Time series of cumulative hydraulic retention time (HRT) of both XLD and XJB reservoirs in the year of 2018; B) Box plot of HRT in both reservoirs (the black lines represented maxima and minima, black squares and middle white lines represented medians and mean values).

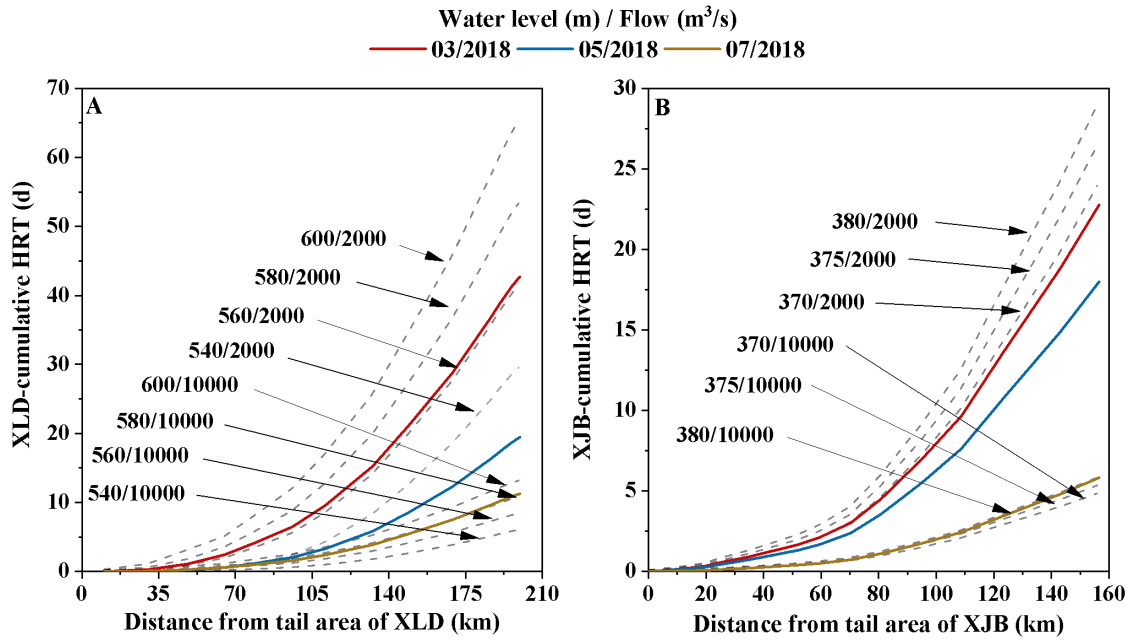


Figure S2. Spatial and temporal variations in the cumulative hydraulic retention time (HRT) with water level and flow in the XLD (A) and XJB (B) reservoirs.

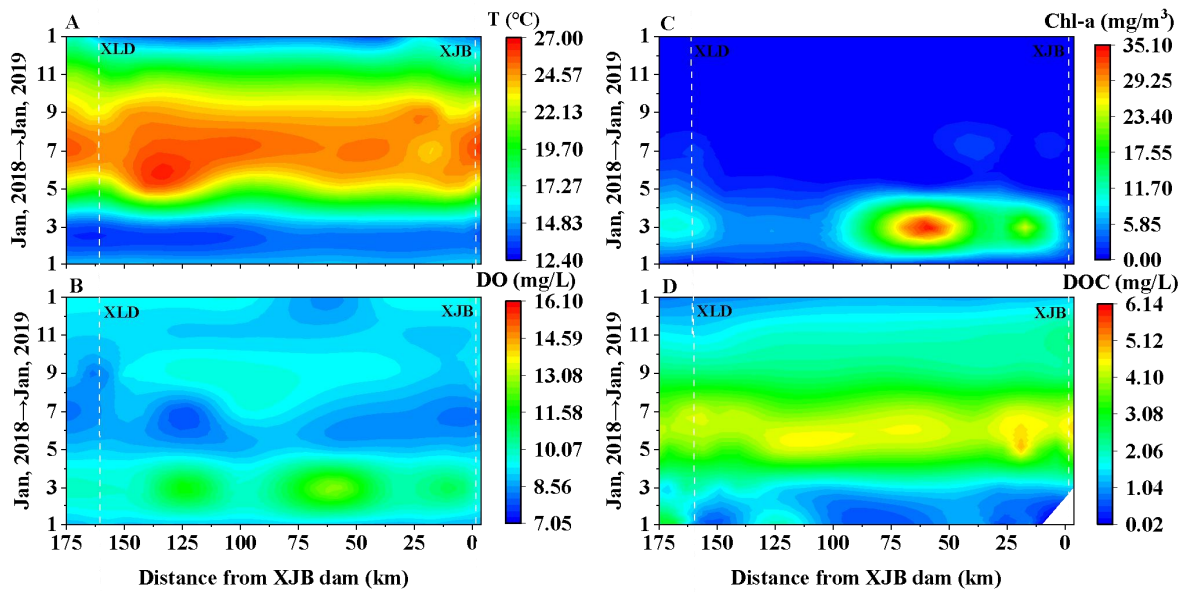


Figure S3. Wavelet figure showing spatial and temporal distributions in water temperature (T, A), dissolved oxygen (DO, B), chlorophyll a (Chl-a, C) and dissolved organic carbon (DOC, D) concentrations in the XLD and XJB reservoirs.

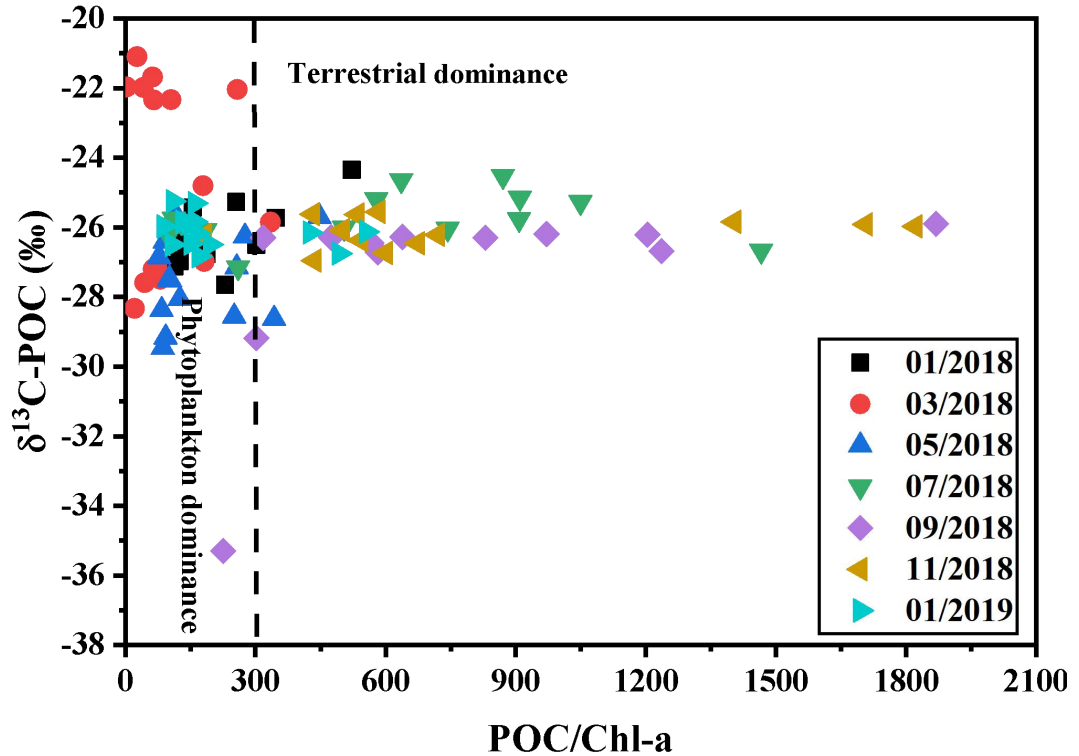


Figure S4. POC/Chl-a ratios vs. $\delta^{13}\text{C-POC}$ in the XLD and XJB reservoirs from January 2018 to January 2019 in the surface water. Symbols below the POC/Chl-a ratio of 300 indicated dominance of phytoplankton of POC, the group with POC/Chl-a ratios above 300 indicated samples with terrestrial dominance of organic carbon (excluding three samples in September and two samples in November with higher POC/Chl-a ratios treated as outliers).

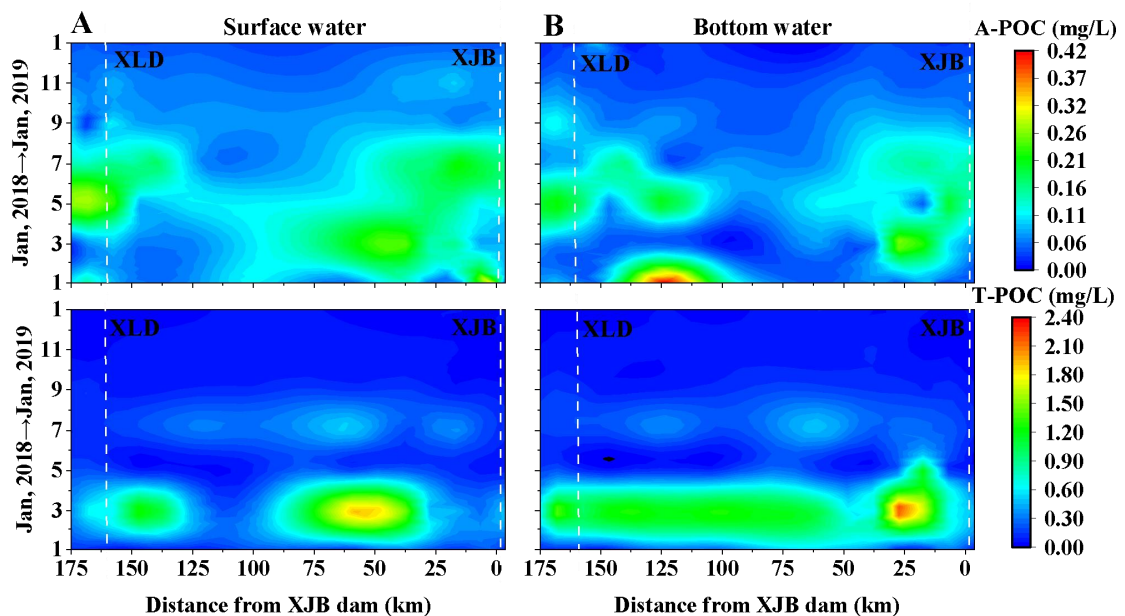


Figure S5. Wavelet figure showing the spatial and temporal distributions in autochthonous POC (A-POC) and terrestrial POC (T-POC) of the surface (A) and bottom (B) water from the XLD and XJB reservoirs.

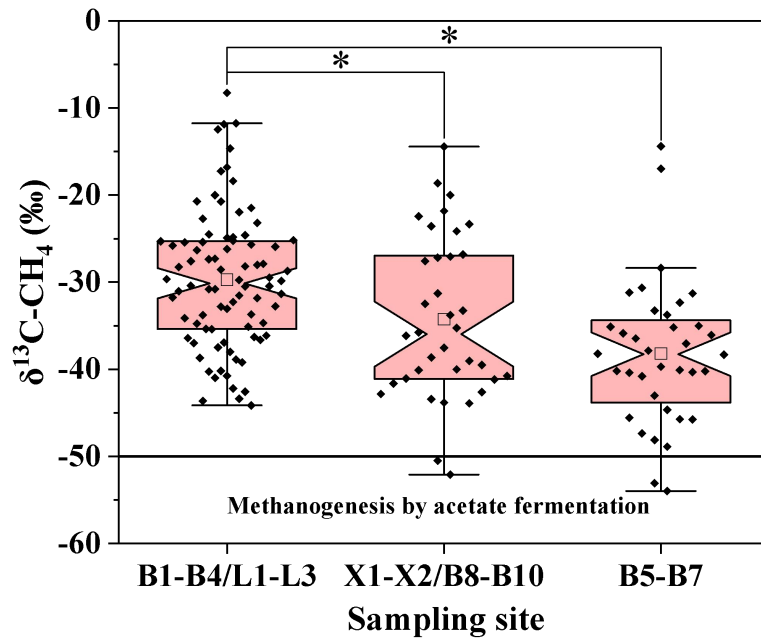


Figure S6. Box plot showing the distribution of $\delta^{13}\text{C-CH}_4$ in different sampling sections from the XLD and XJB reservoirs (the black rhombuses represented $\delta^{13}\text{C-CH}_4$ in all sampling water, black squares and middle notches represented mean values and medians, the vertical and horizontal black lines linking the two boxplots represented significant difference (p -value) by asterisks (* represented $p < 0.05$, ** represented $p < 0.01$, *** represented $p < 0.001$), $\delta^{13}\text{C-CH}_4$ of methanogenesis by acetate fermentation is below the black line at -50‰).

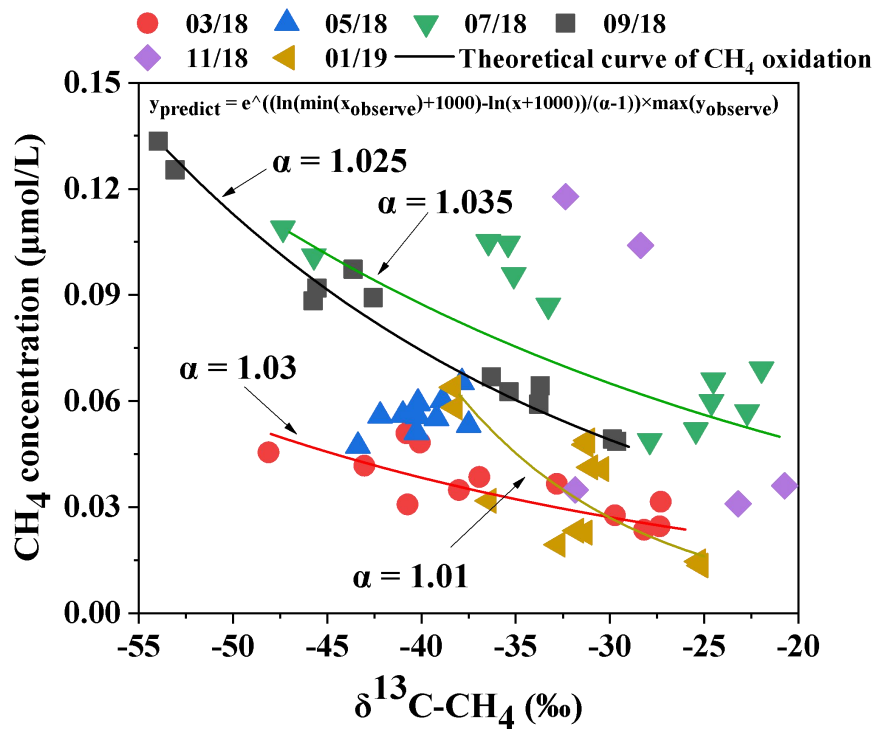


Figure S7. Methane oxidation from B6 to B1 in the XJB reservoir (α is fractionation factor caused by microbial CH_4 oxidation with a range of 1.003 to 1.039 (Templeton et al., 2006)).

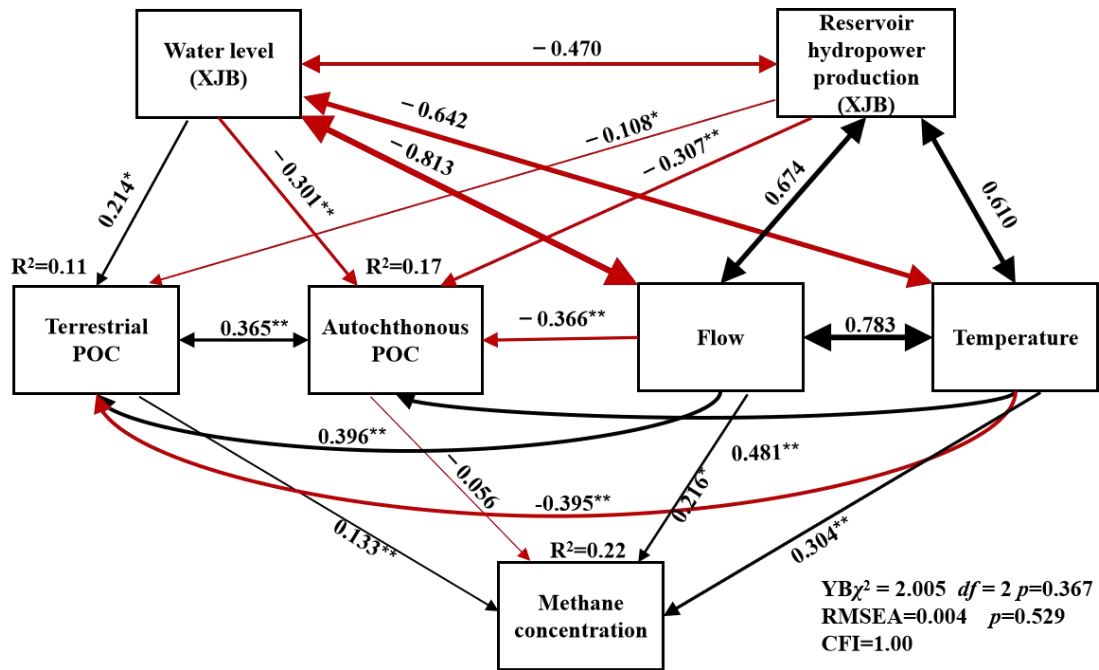


Figure S8. Structural equation model among the water level and hydropower production of the XJB reservoir, water temperature and flow, POC and CH₄ concentrations in the temporal dimension from the XLD and XJB reservoirs. The exogenous variables such as hydropower production and water level of the XJB combining with the water flow, water temperature and water level were used to explain the relationships among endogenous variables as CH₄, autochthonous and terrestrial POC concentrations (the asterisks represented significant difference (p -value, * represented $p < 0.05$, ** represented $p < 0.01$, *** represented $p < 0.001$), black and red arrows with different thickness represented positive and negative relationships from general relationship to significant relationship).

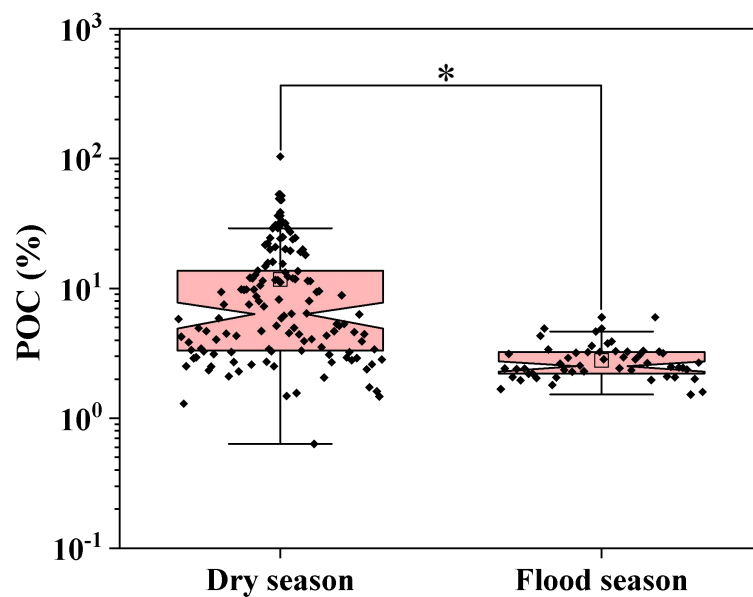


Figure S9. Box plot showing the ratios of POC to TPM during the flood and dry seasons in the XLD and XJB reservoirs (the black rhombuses represented ratios of POC to TPM in different seasons, black squares and middle notches represented mean values and medians, the vertical and horizontal black lines linking the two boxplots represented significant difference (p -value) by asterisks (* represented $p < 0.05$, ** represented $p < 0.01$, *** represented $p < 0.001$)).

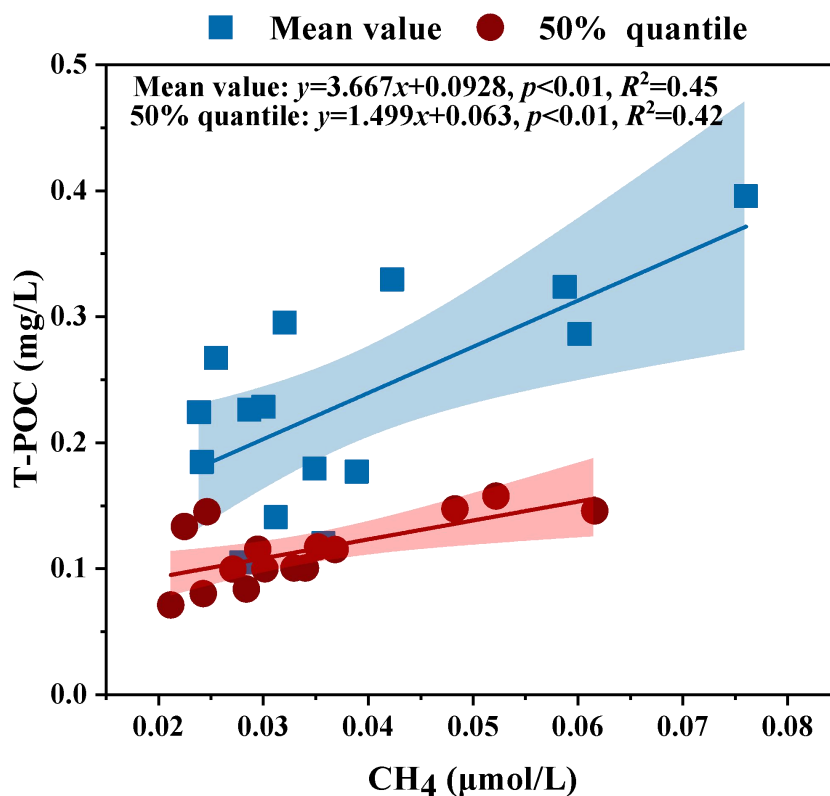


Figure S10. Linear fit relationship between CH₄ and terrestrial POC (T-POC) in the spatial dimension from the XLD and XJB reservoirs (the blue and red area represented confidence bands and confidence level for curves).

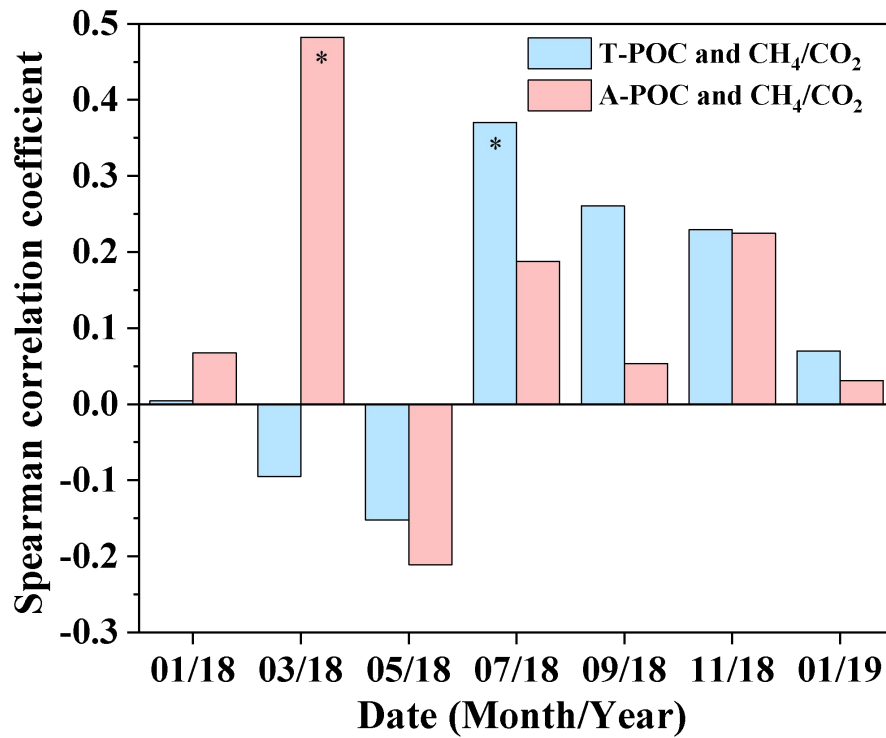


Figure S11. Spearman correlation coefficient of CH₄/CO₂ mole ratio with terrestrial POC (T-POC) and autochthonous POC (A-POC) in the XLD and XJB reservoirs (the asterisks represented significant difference (*p*-value, * represented *p* < 0.05, ** represented *p* < 0.01, *** represented *p* < 0.001).

S2. Tables

Table S1. Parameters of the Xiluodu (XLD) and Xiangjiaba (XJB) cascade reservoirs (Li et al., 2017)

	Xiluodu (XLD)	Xiangjiaba (XJB)
Location of the dam	N28°14'52.81"E103°37'1.59"	N28°38'38.27"E104°23'30.69"
Dam type	Concrete double curvature arch dam	Concrete gravity dam
Maximum dam height	278 m	161 m
Top length of the dam	698.07 m (arch length)	909.26 m
Installed capacity	12600 MW	6400 MW
Estimated annual hydropower production	57.12 TWh ~ 64.06 TWh	30.88 TWh
Reservoir capacity	12.67 km ³	5.163 km ³
Reservoir water level at normal operation (above sea level)	600 m	380 m
Reservoir surface area at normal water level	133.65 km ²	95.6 km ²
Length of backwater area	199 km	156.6 km
Flooded area	125.97 km ²	95.79 km ²

References

- Li, Z., Du, H., Xiao, Y., and Guo, J.: Carbon footprints of two large hydro-projects in China: Life-cycle assessment according to ISO/TS 14067, *Renew Energ*, 114, 534-546, 2017.
- Templeton, A. S., Chu, K.-H., Alvarez-Cohen, L., and Conrad, M. E.: Variable carbon isotope fractionation expressed by aerobic CH₄-oxidizing bacteria, *Geochim Cosmochim Acta*, 70, 1739-1752, 2006.
- UNESCO/IHA: GHG measurement guidelines for freshwater reservoirs, UNESCO, The International Hydropower Association (IHA), 138, 2010.